Energy 346 (2026) 140215

Contents lists available at ScienceDirect

Energy

journal homepage: www.elsevier.com/locate/energy

Evaluating tidal and offshore wind as a sustainable solution for remote off-grid communities

Marianella Bolivar-Carbonell [a,*], Matthew Lewis [b], Roberto Guerrero-Gomez [c], Stephanie Ordonez-Sanchez [a]

[a] Department of Mechanical and Aerospace Engineering, Strathclyde University, Level 8, James Weir Building, 75 Montrose Street, Glasgow, G11XJ, Scotland, UK
[b] Wood Group PLC, Glasgow, UK
[c] MHB Consultants Ltd, Glasgow, UK

ARTICLE INFO

Keywords:
Tidal stream currents
Data-assimilative model
ADCP
Arctic
Remote off-grid
FES2014

ABSTRACT

Locating renewable energy systems in remote areas with extreme conditions is challenging due to weather variability and past deployment failures. This study assesses tidal and offshore wind resources for application in off-grid communities, focusing on data accuracy and site viability. Tidal energy, being highly predictable, is analysed using ADCP measurements and the FES2014c model at sites in the North Atlantic, including the FoW (Orkney, Scotland) and the Nares Strait (Canadian Archipelago), to understand any limitations with the use of FES2014c in the area evaluated. Strong correlations (R^2 = 83%–89%) were found, although bathymetry-related errors were noted in shallow areas. FES2014c was then used to evaluate Nunavut locations where tidal or offshore wind energy could be used to reach net-zero targets. In Nunavut, Canada, correlations between the MERACAN Atlas and the FES model varied widely (R^2 = 19%–95%), with skill scores between 39%–94%. The FES model showed deviations from 1.12 ms-1 to 0.03 ms-1, while tidal amplitude remained reliable, aiding site identification. A site in Naujaat was identified as a suitable location for the deployment of both tidal and offshore wind energy, with estimated capacity factors of 38% for tidal and 28% for wind. The combined annual energy production is approximately 1791.8 MWh. However, for offshore wind development only, no suitable locations were found where bathymetric conditions matched with capacity factors. In contrast, tidal stream analysis identified at least four viable turbine sites, each with a capacity factor exceeding 20%.

1. Introduction

1.1. Identification of suitable energy sites in Nunavut, Canada

Much research has focused on reducing the cost associated with Gigawatt scales of renewables for national electricity distribution systems. However, ~40% of the world is classed as "being in energy poverty" with ~13% (>5 billion people) still having no access to electricity [1]; for example, Indonesia alone has 13,000 rural communities without utility power services [2]. Renewable energy offers a sustainable pathway for improving access to low-carbon electricity (e.g. [3,4])10, but also powering systems essential for communities, such as desalination for drinking water (e.g. [2]). Of these renewable energy markets, remote communities and industries are already paying a high price for imported diesel to run generators in local-scale systems. For example, over 20 million people, inhabiting over 1800 islands, are paying up to €2000/MWh [4], and an analysis shows a ~20% reduction in cost with renewable energy systems [5]. The reason for such high energy costs in remote and developing island communities is the 500–2000 Euros-per-MWh costs for importing diesel, as "fuel imports are often 200%–300% above world market rates,[6]. Indeed, a 2018 Castalia Advisory Group's report into energy for the state of Micronesia, revealed ~67% have access to electricity currently paying ~410–460 USD/MWh, with only 19% from renewables and 4.2M gallons of diesel imported and multiple 3–4 MW batteries at each island for supply–demand balancing; whilst in the Canary Island, 99% of energy comes from imported diesel (7% electricity from renewables) to the 2.2M residents [7]. Therefore, renewable energies offer a cost-effective and sustainable pathway to reducing energy poverty and improving electrification rates; however, for any electricity distribution network, demand must be balanced by supply.

Nunavut in Canada is as remote as island communities, and because of their exposure to the extreme environment, they rely heavily on fossil fuels. The Nunavut Settlement Area encompasses 20% of Canada's

* Corresponding author.
E-mail address: marianella.bolivar-carbonell@strath.ac.uk (M. Bolivar-Carbonell).

https://doi.org/10.1016/j.energy.2026.140215
Received 19 August 2025; Received in revised form 27 November 2025; Accepted 26 January 2026
Available online 28 January 2026

landmass, making it the country's largest jurisdiction, spanning approximately 2,132,780 $1\,km^2$. According to the 2016 Census data from Statistics Canada, Nunavut has an estimated population of 40.000 inhabitants. More than 80% of this population is Inuit, residing across 25 municipalities within three distinct regions: Qikiqtani (Baffin), Kivalliq, and Kitikmeot. Possibilities of harvesting energy from rivers, wind and solar are being explored to help decarbonise those communities [8]. However, given the vast coastal area in Arctic Canada, marine renewable energy systems like offshore wind and tidal stream around Nunavut could offer an option to reduce the dependence on fossil fuels.

Specifically, Nunavut alone has a tidal energy potential of over 30,000 MW from 34 sites [9,10]. There is growing interest from developers and start-up companies to generate 10 MW of electricity in Iqaluit using underwater turbines in Frobisher Bay [10]. This energy could support the necessary harvesting infrastructure development while also providing enough for export [9–11]. As a result, it can assess various advantages and applications of this resource, including power generation, water pumping, desalination [12], and aquaculture [13].

1.2. Assessing tidal stream resource

To assess the tidal energy potential, techniques such as field observations, data analysis, and numerical modelling have been used [14]. However, tidal energy data cannot be easily accessed like offshore wind data, which is more readily available and widely validated [15–17].

In-field observations on tidal currents are limited because accurate measurement requires tidal current sensors, e.g., Acoustic Doppler Current Profilers (ADCPs). These devices are expensive and require skilled personnel for their operation and maintenance. Furthermore, the duration of measurements is limited due to the battery and access to data storage can be restricted due to concerns about data privacy or security.

The latter led to the development of various methods for estimating current velocities using numerical modelling, especially for tidal stream energy resource assessment [18–20]. These models are presented in three different forms as follows [21–25]: **Hydrodynamic models**, which utilise equations of motion and consider the astronomical tidal potential, **Empirical models**, based on harmonic constants derived from satellite data, and **Data-assimilate models**, which combine information from both sources.

The initial hydrodynamic and empirical models were commonly used to understand the horizontal flow, focusing on analysing the M4 and M2 harmonics, as demonstrated by Davies et al. (1986) and (1992) [26,27]. They demonstrated a fully non-linear three-dimensional hydrodynamic model for tide elevations and currents, using a finite-difference grid horizontal and the Galerkin method in the northwest European Continental Shelf. Comparisons from the frequency and temporal analysis of the M4 component elevations and currents with observations at various locations were made by calculating the ellipses for the seabed and surface, amplitude and phases for each component, respectively. They concluded that some changes in the physics and a finer mesh in a new model would correctly reproduce the generation and dissipation of the M4 tide in particular regions in the northwest European Continental Shelf.

Luyten et al. (1991) [28] compared M2 tidal currents obtained from moored current measurements with the Schiwiderski model and concluded that hydrodynamic models can perform better under specific local conditions while remaining computationally efficient. However, they noted that these models do not assimilate observational data to refine predictions and may be more sensitive to initial errors and boundary conditions.

This limitation is also supported by more recent studies, including Xiaodong Liu et al. (2021), Yi Wen et al. (2022), Peng Dai et al. (2023), and Jian Chen et al. (2024) [29–32], where hydrodynamic models such as MIKE21, MIKE 3D, FVCOM (Finite Volume Community Ocean Model), and POM (Princeton Ocean Model) were implemented to assess tidal stream energy potential. In many cases, these models were particularly useful for resource evaluation in small areas with low tidal current velocities. Their application is especially relevant in narrow channels or regions with complex hydrodynamics, where capturing turbulence, localised flow gradients, and other fine-scale processes is crucial for identifying suitable sites for tidal energy deployment.

Nevertheless, data-assimilative modelling approaches have the advantage of incorporating observational datasets to improve predictive accuracy and provide a more robust representation of complex ocean processes, while being less computationally expensive compared to the hydrodynamic models mentioned before and thus being useful for an initial site selection.

Consequently, Dushaw et al. (1997), Egbert et al. (1994) and Ray et al. (2001) [25,33,34] investigated currents of various tidal constituents in version 2.0 of the TOPEX/POSEIDON (TPXO) model, creating the first data-assimilative model. All these studies focused on the barotropic component of tidal currents. They derived currents from acoustic tomography and moored current meters, helping to determine tidal currents from altimetrically derived tidal elevations. Most barotropic tidal models do not solve for the currents directly; rather, they use mass transport equations to derive the magnitude and direction of the currents. The accuracy of the model depends on the seafloor topography employed and is not constrained by observations, making it inherent to hydrodynamic models.

Tidal analysis and prediction were extended to include other tidal components. This expansion allows a better understanding and modelling of sediment movements in large-scale studies of continental shelves according to Walton et al. (2002) and Lyard et al. (2006) [19,35]. Also, Neil et al. (2010) [36] conducted a study analysing sediment erosion and deposition's spatial and temporal distribution over shelf seas spanning 12,000 years. As part of their research, they developed a tidal and wave model. In the tidal modelling component, the model output was compared with the FES2004 model [19]. The results showed good agreement across the domain in terms of elevations and currents for the semi-diurnal tidal constituents (M_2, S_2, M_4, N_2, K_1, O_1), incorporating a non-linear enhancement to account for wave–current interaction.

These models have been continuously updated with data from the TOPEX/ Poseidon satellite altimetry series since 1993, and are designed to predict both water levels and currents. The TOPEX model has demonstrated greater accuracy in deriving water elevations and currents, improving consistency with moored observations in these areas. However, while the authors claim that the model is accurate for deeper waters, they do not specify the depth limits for its effectiveness [37]. But they provide an effective means of investigating the fundamental characteristics and general patterns of tidal currents at various spatial and temporal scales.

Comparisons of modelled tidal currents with observations are much less common than comparisons of tidal elevation observations, especially on the basin and global scales. The accuracy of state-of-the-art global barotropic tide models was assessed by Stammer et al. (2014) [37]. Over 20 years in a study of bottom pressure data, coastal tide gauges, satellite altimetry, various geodetic data on Antarctic ice shelves, and independently tracked satellite orbit perturbations were used, it was concluded that the accuracy remains problematic due to the relative sparseness of in situ velocity measurements and the difficulty of isolating the barotropic mode in moored current meter measurements.

Later, Ranji et al. (2017) [38] conducted a comprehensive comparison of different tide models to evaluate their accuracy in predicting tidal levels, currents, and velocities in the Persian Gulf and Oman Sea. It was found that among all the compared models, the Finite Element Solution (FES) model (version 2012) stood out for its superior accuracy in predicting tidal levels and currents across both regions. The study highlights the importance of the number of constituents included in a

model, particularly for shallow water tidal constituents, in enhancing prediction accuracy.

Further analysis within the study reveals that while the FES12 model excels in predicting tidal levels, it shows discrepancies in predicting tidal currents due to atmospheric pressure disturbances. Although the FES model provided the best fit among the models assessed according to various statistical measures, the results highlighted the complexity of tidal dynamics in the Persian Gulf and Oman Sea, especially in shallow water regions where maximum prediction errors were observed [38].

Cancet et al. (2017) and Lyard et al. (2021) [20,39] validated forty-eight ADCPs data sets in the Australian continental Shelf with FES2014. It was concluded that continued validation and comparison of this type of model are essential. The study highlighted the model's sensitivity to uneven local bathymetry and shallow areas, where the resolution may be insufficient to properly resolve the currents. All the above involve that it is imperative to continue validating the model for the currents, and to enhance prediction accuracy in both deep and shallow water areas, it is essential to calibrate and refine this model [19,28,37,40–42].

Recently, Loc Nguyen-Xuan (2024) conducted a regional assessment of six data-assimilative tidal models, including FES2014, to quantify the tidal energy resource in the Vietnam East Sea (VES). Model accuracy was evaluated using a Taylor diagram in combination with root-mean-square deviation (RMSD) metrics to quantify agreement with in-situ tide-gauge observations. Among the tested products, FES2014 exhibited the highest match, which is attributed to its advanced multi-source data assimilation framework, flexible mesh configuration, and enhanced capability to reproduce complex coastal hydrodynamics. The study highlights the need to validate global tidal products regionally, as model performance can vary substantially with local bathymetry, boundary forcing, and coastal morphology. They noted that these results provide a baseline for subsequent high-resolution modelling efforts, including localised hydrodynamic simulations and site-specific tidal stream resource assessments.

Identifying and refining the use of FES2014c has opened up opportunities to explore new areas that currently rely on fossil fuels, such as remote communities. In particular, this supports the development of marine renewable energy sources like tidal currents, due to the lack of research on the topic. Focusing on Nunavut, the application of FES2014c can go beyond resource analysis by helping to determine which types of tidal energy devices could be installed at key initial locations. This approach could also be extended to other regions to assess energy access, evaluate marine energy potential, and identify new areas for exploration.

Building on the significance of the current literature, the research aims are:

- To evaluate for the first time the accuracy of a global assimilative tidal model at regional scales in Scotland and Arctic Canada. This was done by comparing FES2014c with ADCP observations and evaluating it using a harmonic tidal analysis that accounts for dissipation, non-linear friction, and shallow-water dynamics.
- To identify suitable areas in Nunavut where tidal energy could be used to reach net-zero targets, with wind energy considered as an alternative or complementary option. This objective was met by estimating annual power generation using data from the validation of FES2014c and offshore wind data from ERA5 [43], to assess whether tidal, wind, both, or neither is most suitable for the region.

2. Methodology

2.1. Identification of suitable energy sites in Nunavut, Canada

In this research, a decision-making criterion was designed to identify suitable locations for the development of marine energy, specifically for tidal stream and offshore wind in the Nunavut area. The suitability of the criteria of tidal stream and offshore wind is mainly related to the resource, oceanographic features, and technical characteristics of device, as observed in Table 1. A flowchart describing the steps of the methodology can be seen in Fig. 1.

2.1.1. Resource features

Assessing tidal stream resource Alternative approaches were explored to evaluate remote locations in Nunavut where ADCP data is lacking. The Marine Energy Resources Atlas of Canada (MERACAN) emerged as a promising tool for providing tidal current information in this area, where ADCP data are absent, and was developed by the National Research Council. The map shows tidal flows and hydrokinetic energy in proximity to communities in northern Canada. This application allows users to investigate and assess potentially exploitable tidal energy resources by providing spatially and temporally varying data, including tidal height, currents, seabed elevation, and annual energy production [48]. However, this model has some limitations, including high uncertainty due to the lack of field data and the absence of high-resolution modelling and specific regional studies. This can introduce significant errors in areas with narrow coastal channels, as described in [48]. Thus, part of this research builds on the analysis conducted by MERACAN to assess the viability of tidal sites in the Arctic regions of Canada and to analyse them with FES2014c.

Validation of data assimilation model The FES2014c tidal prediction model was selected, featuring C and Python Application Programming Interfaces (API), which provide functions for computing elevations and currents on the eastward and northward vectors. The model has a resolution of 1/16 degrees. Compared with other models, this software includes 34 tidal frequencies, including several long-period tides, minor diurnal, and semi-diurnal tides, and nonlinear overrides (See Table 2).

The model employs a 20-year time series of altimeters to enhance bathymetry and achieve greater resolution in shallow and transition water areas defined in Table 3. It incorporates all pertinent variables derived from the mission of the altimeter data into a hydrodynamic model based on the tidal equations of Laplace. In addition, it assimilates a substantial portion of coastal and deep-ocean data from tide gauges, ensuring a comprehensive representation of the available information.

To ensure the suitability of the FES global tide model for regional-scale resource assessment in Nunavut, a validation with the data assimilation model step was required before it is applied for tidal energy resource assessment. The literature consistently highlights the need for regional validation when using global tide models in complex hydrodynamic environments, especially when assessing tidal stream energy potential. Most existing studies have focused on tidal elevation validation, while limited work has evaluated tidal currents, which are essential for energy extraction analysis. Therefore, the model was validated against independent ADCP current measurements from Scotland and Canada with different tidal regimes. Scotland was chosen due to the availability of high-quality ADCP data compared to the data found in Arctic Canada. These datasets are neither derived nor assimilated into the FES model, ensuring a neutral evaluation of its performance. Establishing reliability in these independent locations provided the necessary confidence to apply the model to Nunavut, where in situ current observations are scarce. Complementary cross-validation against the MERACAN Atlas further supported the robustness of the modelling approach.

Time domain analysis To compare the FES2014 data against the existing ADCP data sets, a number of metrics were employed based on the work proposed by [26,27,49–53] and are defined as follows in Table 4 where $\hat{y}_i$ is the estimate data and y_i is the observed data.

Table 1
Criteria for identifying suitable wind and tidal energy sites in Nunavut, Canada.

Criteria	Subcriteria	Requirements	Type
Resource	Minimum fluid velocity[a]	Wind ≥ 2.5 ms^{-1} Tidal ≥ 0.4 ms^{-1} [44]	Both
Technical	AEP (per turbine) CF (per turbine)	Based on velocity + turbine size Wind: 35%–40% [45] Tidal: 16%–42% [44,46]	Both Both
Oceanographic	Bathymetry	Wind: 10–50 m (fixed) Tidal: 18–50 m (fixed), >4 m (float) Clearance: 5 m seabed, 8 m surface	Fixed/Float [47]

[a] This velocity is related to the cut-in velocity of the device. Details of specific turbines used in this study can be seen in Tables 5 and 6.

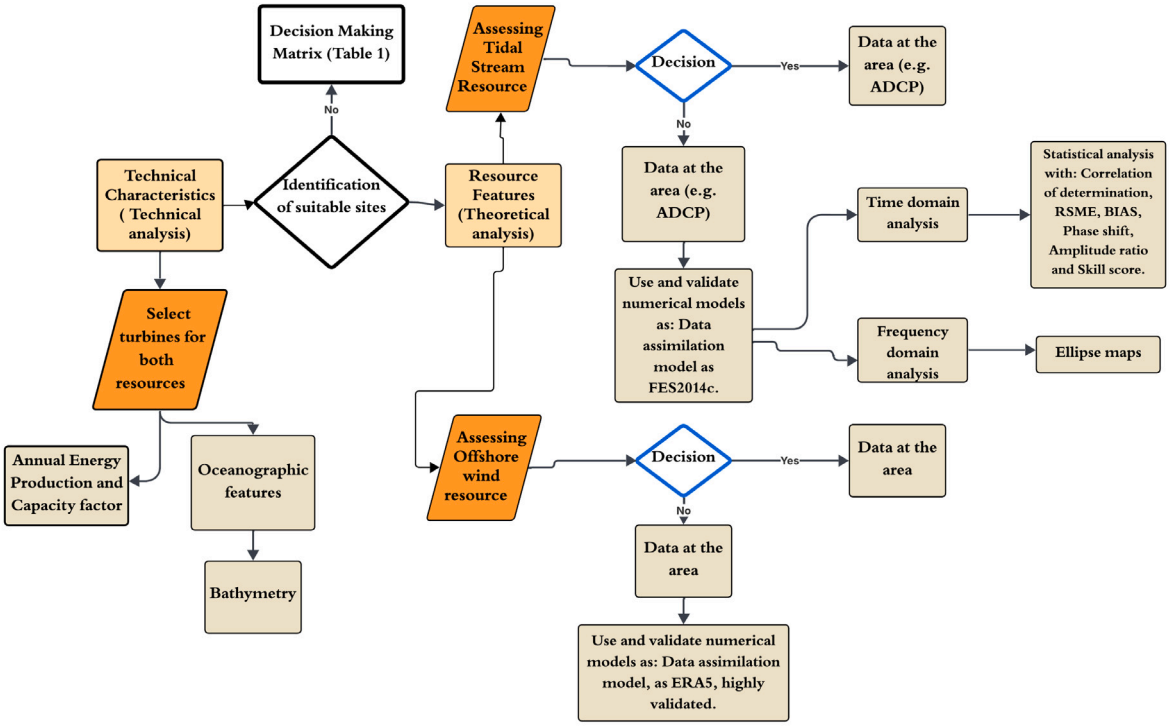

Fig. 1. Flowchart - Main methodological steps for decision-making matrix on Table 1.

Table 2
Barotropic tide model summary.

Model	Tidal constituents	Grid	Authors
FES2014c	Q_1, O_1, P_1, K_1, S_1, N_2, M_2, S_2, K_2, $4M_4$, ($2N_2$, MN_4, MS_4), [S_a, M_m, M_f, MS_f, Mt_m, MSq_m, J_1, ε_2, μ_2, ν_2, MKS_2, λ_2, L_2, T_2, R_2, M_3, N_4, S_4, M_6, M_8]	1/16°	Lyard et al.; Carrère et al. (2016)

Table 3
Water depth classifications (Musial & Butterfield, 2004).

Classification	Depths
Shallow water	0–30 m
Transition water	31–50 m
Deep water	≥50 m

Frequency domain analysis The research was then conducted on a frequency domain analysis to verify the FES2014c capabilities against the ADCP datasets. The analysis focused on vectors using harmonic analysis, performed with the T-TIDE package [54] in each current direction (eastward and northward). Then, the in situ data (ADCP) was compared to FES2014c in terms of tidal current ellipse characteristic differences, based on the work of Griffin et al. (2021), Lyard et al. (2020) and Stammer et al. (2024) [19,37,39,55]. A synthetic description of the tidal currents for a given tidal component (M2) is given by this analysis which complements the time domain data outputs and ensures a full quantification of the models against experimental data.

The length of the semi-major axis gives the maximum amplitude of the tidal current and the orientation of the ellipse gives the angle between the main current direction in the eastward direction. The parameters of the ellipse as orientation and length of the minor and major axes, are computed from tidal harmonic constituents estimated in both directions.

Table 4
Statistics: Statistical metrics used for model accuracy.

Statistic name	Equation	Expected range	Success metric
Coefficient of determination (R-squared)	$R^2 = 1 - \frac{\sigma_r^2}{\sigma^2}$	$0 \leq R^2 \leq 1$	Higher values indicate better agreement (≥ 80%).
Root Mean Squared Error (RMSE)	$RMSE = \sqrt{\frac{\sum_{i=1}^{n}(\hat{y}_i - y_i)^2}{n}}$	$RMSE \geq 0$	Lower values indicate higher accuracy.
Bias	$BIAS = \frac{\sum(\hat{y}_i - y_i)}{\sum y_i}$	Ideal = 0	Overestimation (positive) or underestimation (negative).
Nash–Sutcliffe Efficiency (NSE)	$NSE = 1 - \frac{\sum(\hat{y}_i - y_i)^2}{\sum(y_i - \bar{y})^2}$	$-\infty < NSE \leq 1$	Values near 1 indicate excellent performance.
Phase shift (cycles)	$Phase = \frac{\phi_y - \phi_{\hat{y}}}{2\pi}$	Ideal = 0	Temporal shift between observed and predicted time series.
Amplitude ratio	$Amplitude\ Ratio = \frac{Amp_y}{Amp_{\hat{y}}}$	Ideal = 1	Values near 1 indicate good amplitude representation.
Skill score	$Skill_{score} = \sum_{i=1}^{n} \min(Z_{\hat{y}_i}, Z_{y_i})$	$0 \leq Skill \leq 1$	A value of 1 indicates a perfect match (≥ 70%).

The 34 tidal constituents, as in the time domain analysis, were used as the basis for the model-ADCP comparisons presented in this study, which are focused on the results of M2 as the principal harmonic after the signal-to-noise power ratio (SNR) with the five main constituents of each dataset.

The model error for amplitude and phase was calculated for each dataset for the M2 constituent. The root mean square error (RMSE), as defined in the time-domain analysis (Table 4), was computed. The tidal current ellipses were computed from the current meter observations (ADCP) in red and from the FES2014c in blue. These ellipses were displayed for the M2 tidal component, along with the statistical analysis proposed.

Assessing offshore wind resource To analyse the opportunities of decarbonisation using alternative and more developed technologies, the sites analysed for tidal stream resources were compared to offshore wind data. The data was examined with a reanalysis dataset, ERA5, that provides wind data for long-term duration with different spatial and temporal resolutions globally and is easy to access and broadly validated [17,56–62]. The ERA5 reanalysis model integrates data with global observations. It is also a data assimilation model based on methods used by numerical weather prediction centres, but with a reduced resolution to allow for the incorporation of improved versions of the original observations. For this study, the 'ERA5 hourly data on single levels from 1940 to present' dataset was used, providing hourly estimates for many atmospheric, ocean–wave and land–surface quantities. The data is gridded to a regular latitude–longitude grid of 0.25 × 0.25 degrees for the atmospheric reanalysis and downloaded at 10 m to be extrapolated to the heights of the selected turbines for this study, as is shown in the equation for power law in wind profile, where V is the wind speed at height z, V_{ref} is the wind speed at the reference height z_{ref}, z is the height above ground level, z_{ref} is the reference height and α is the power-law exponent.

$$V = V_{\text{ref}} \left(\frac{z}{z_{\text{ref}}} \right)^{\alpha} \tag{1}$$

2.1.2. Technical characteristics

Annual energy production and capacity factor The annual energy production is quantified according to EMEC (2009) and Lewis (2021) [44,53] and which informed the selection of the most suitable site for deploying wind and tidal turbines in Nunavut, Canada. The datasets for each resource were downloaded: offshore wind, from ERA5, [43] for 4 years (2020–2024), and tidal stream, from FES2014c [20] for 1 year (2024). A selection of turbines and peak performance operations were studied, based on the velocity exceedance curves and by performance (Cp vs. TSR (Tip Speed Ratio)), described in Tables 5 and 6.

Table 5
Description of the selected offshore wind turbines for the assessment.

Parameters	0.5 MW	1.0 MW
Rated speed (ms^{-1})	12	15
Cut-in speed (ms^{-1})	2.5	3.0
Cut-out speed (ms^{-1})	25	25
Rotor speed (rpm)	38	22
Rotor diameter (m)	40.3	54.2
Reference	[63]	[64]

Table 6
Description of the selected tidal stream turbines for the assessment.

Parameters	Tocardo 42 kW–55 kW	Rivgen 25 kW	Tidgen 200 kW
Rated speed (ms^{-1})	2.0–2.5	2.25	2.25
Cut-in speed (ms^{-1})	0.4–0.5	0.5	0.5
Cut-out speed (ms^{-1})	2.6–3.8	3.0	3.5
Rotor speed (rpm)	32–39	2.25	2.25
Rotor diameter (m)	6.3–5.1	–	–
Rotor ratio (m)	–	1.5	x8(1.1)
Rotor length (m)	–	10.36	x8(6.25)
Reference	[65] [66]	[67] [68]	[69] [70] [71]

To understand the potential for power extraction in an area by selected turbines and ensure that the tidal and offshore wind resources available are not over-extracted, the velocity distribution was calculated. The analysis of the velocity distribution (exceedance curve) was obtained using a bin size defined by Sturges Law and standard intervals of 1 h for each dataset and resource. Once the velocity distribution was calculated, it was applied to each power curve to estimate the annual energy output. This considers the characteristics of the devices that were extracted for each turbine (Eq. (2)). The expected annual energy contribution (AEP), in kWh, for a device with a defined power curve, was obtained by combining the power curve with the frequency distribution of the velocity for each site (Eq. (4)), where the Pmean is the power in kW generated by velocity bin of the power device curve [53]. The annual energy output (AEP) divided by the maximum possible output ($P_{nominal}$) from the device will give us the capacity factor, CF (Eq. (3)). Power represents the rate at which energy is transferred. To determine the amount of energy produced over a given period, the power time series is integrated. The result is typically expressed in energy units such as GWh. For example, integrating the power output over one year provides the Annual Energy Production

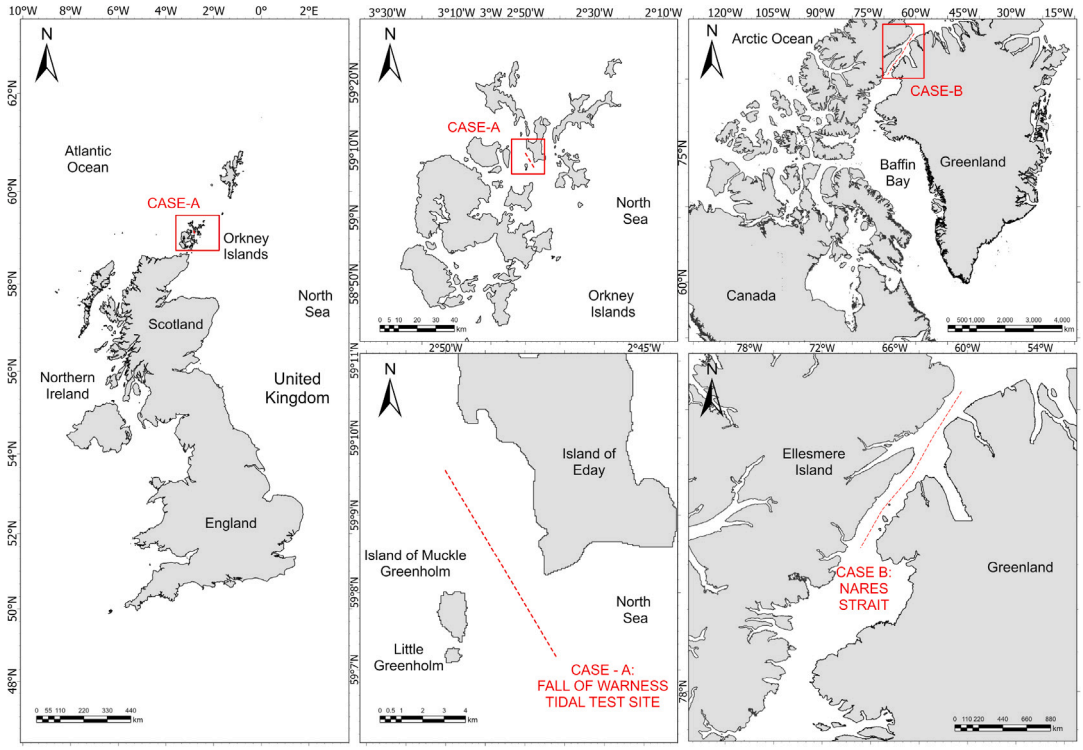

Fig. 2. Study area. Case A. FoW, Scotland, and Case B. Nares Strait, Canada.

(AEP) in GWh.

$$P_{KE} = \frac{1}{2}\rho A V^3 Cp \tag{2}$$

$$CF = AEP/P_{nominal} \tag{3}$$

$$AEP = 8760 P_{mean} \tag{4}$$

2.1.3. Oceanographic parameters

Bathymetry The bathymetry was downloaded from General Bathymetric Chart of the Oceans (GEBCO) [72] (See Figs. 5 and 6). The bathymetry is important as a technical criterion for the requirements of installation and operational maintenance of offshore wind turbines and tidal stream turbines, as shown in Tables 6 and 5.

3. Results and analysis

3.1. Data assimilation model validation for tidal current analysis

The areas considered in this study for comparison of the FES model were the FoW in the Orkney Islands, Scotland (Case A) and the Nares Strait (Case B). The FoW and the Nares Strait were selected because of the availability of data to validate the model. The areas considered for investigation of site selection for decarbonisation were assessed based on existing settlements in the area, as shown in Fig. 2.

In the FoW, ADCP data were extracted from the ReDapt [73] and the EPSRC DYLOTTA [74]. The data points covered periods from 2013–2014 and 2005–2009, respectively, with sample frequencies of 1 h, 10 min, and 6 min by DYLOTTA and 5 min by ReDAPT, with a total of 29 data points. The FoW data was grouped into 3 subgroups according to their proximity, and as shown in Table 7. Average bathymetry records can be seen in Fig. 3 for each location.

The data points from the Nares Strait between Canada and Greenland were obtained from the National Science Foundation and the University of Delaware through the Arctic Data Centre [76,77]. The data cover periods from 2003–2009, respectively, with sample frequencies of 30 min, with a total of 9 data points. Due to the location of each data point, it was not feasible to group points for analysis like the FoW case. The depths of the site assessed were generally in a range between 157 m and 366 m according to Fig. 3 compared to the FoW area, with relatively shallow areas (see Table 8).

Table 7
Description of the bathymetry and temporal resolution in FoW area.

Groups	Surveys	Depths	Temporal resolution	Reference
Group 1	a	31 m	2.3 months	[75]
	b	27 m		
Group 2	a	15 m	0.5 months	[75]
Group 3	a	43.1 m	14.5 months	[73]
	b	42 m		
	c	42.2 m		
	d	36.2 m		[75]
Group 4	a	42.55 m	3.7 months	[75]
	b	37 m		
	c	42 m		
	d	40 m		

3.2. Time domain and frequency analysis

As mentioned before, to assess the accuracy of the model analysis for several tidal energy resource zones, areas in Scotland and Canada were used to validate the reliability of the analysis method presented in this paper. Once the validation was completed, FES2014 was used to identify suitable tidal sites in the Nunavut region of Canada.

Case A - FoW Statistical indices were extracted for eastward and northward velocities and are presented in Table 9 for the FoW scenario.

Eastward component Group 3 has the highest correlation coefficient among the groups, with R^2 at 0.83. This indicates that the model explains a significant portion of the variability in the data, suggesting a strong linear correlation. The average error, measured as RMSE, is

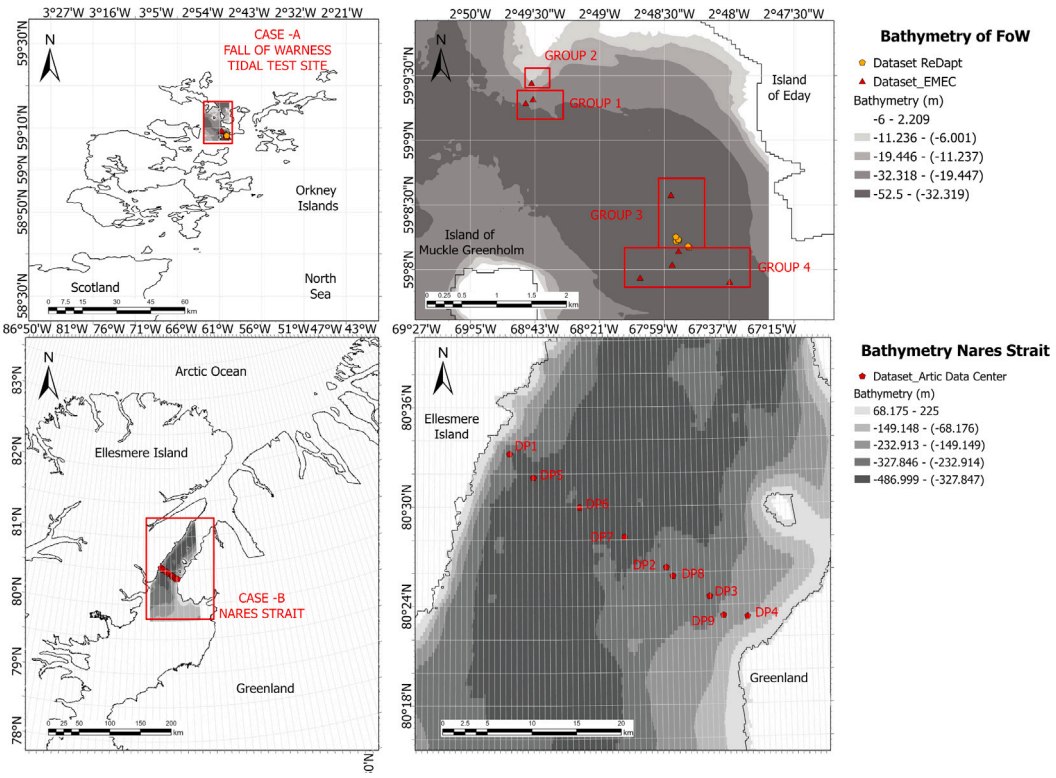

Fig. 3. Bathymetry Map and Survey points from ADCP - FoW and Nares Strait.

Table 8
Description of the bathymetry in the Canadian Archipelago area.

Datapoints	D1	D2	D3	D4	D5	D6	D7	D8	D9
Depths (m)	302 m	299 m	263 m	157 m	366 m	358 m	356 m	294 m	228 m

Table 9
Results of statistics for FoW scenario.

Components	Statistic	Group 1	Group 2	Group 3	Group 4
Eastward component	R^2	0.73	**0.40**	**0.83**	0.80
	RSME (ms^{-1})	0.65	**0.95**	**0.54**	0.57
	Max - Min (ms^{-1})	[1.85 - (−2.28)]	[2.37 - (−3.93)]	[2.72 - (−2.90)]	[2.14 - (−3.26)]
	BIAS (ms^{-1})	0.85	**0.62**	**0.92**	0.91
	Skill score	**0.58**	0.59	**0.80**	0.79
	NSE	0.61	**0.24**	**0.74**	0.73
	Phase shift (cycles)	**0**	**0**	**0**	**0**
	Amplitude ratio	1.44	**2.24**	**0.99**	0.77
Northward component	R^2	**0.82**	**0.62**	0.70	0.63
	RSME (ms^{-1})	**0.65**	0.90	0.87	**0.98**
	Max - Min (ms^{-1})	[2.68 - (−3.03)]	[3.21 - (−4.09)]	[3.38 - (−4.09)]	[3.20 - (−4.14)]
	BIAS (ms^{-1})	**0.92**	**0.79**	0.84	0.80
	Skill score	0.77	0.77	**0.70**	**0.81**
	NSE	**0.77**	**0.53**	0.66	0.60
	Phase shift (cycles)	**0**	**0**	**0**	**0**
	Amplitude ratio	1.24	**1.76**	1.45	**1.18**

0.54 ms^{-1}, and the NSE value is close to unity at 0.74, supporting good model performance. However, a BIAS value of 0.92 ms^{-1} suggests that the model tends to overestimate the data, given that an optimal value close to zero was expected (see Table 9).

The amplitude ratio in the eastward direction exhibits a value close to unity (0.99) and shows no lags. The statistics also suggest that FES2014c, in this group, can simulate the observed conditions 80% of the time, as indicated by the skill score (see Table 9).

Group 2 has an R^2 of 0.40. This indicates that the model simulates only a moderate portion of the velocity. Consequently, the RMSE of 0.95 ms^{-1} suggests that, on average, the observed values vary from a minimum of −3.92 ms^{-1} to a maximum of 2.37 ms^{-1}, indicating a range of values the model cannot fully capture. Additionally, the NSE value of 0.24 is only as reliable as the average of the observations, given that it is close to zero. The model also overestimates the dataset by 0.62 ms^{-1}.

Regarding the amplitude ratio and phase shift values in Group 2, the model exhibits a proportion of 2.24, with the highest amplitude ratio in the eastward direction but without lags as compared with Group 3. However, the skill score is the lowest, at 59%, indicating little to no match between the model and the dataset.

Northward component Group 1 exhibits a similar behaviour to Group 3, with comparable directions between the ADCP data and the model. This similarity is supported by a high R^2 correlation percentage of 82%, a low RMSE of 0.65 ms^{-1}, and a northward velocity overestimation of 0.92 ms^{-1} as indicated by the BIAS with a Nash–Sutcliffe efficiency coefficient (NSE) value for Group 1 of 0.77, close to the unity, that indicates the good correlation between the model and the dataset.

Moreover, we conducted an analysis comparing the amplitude ratio and phase shift between the observed and modelled data sets. It was found that, in Group 1, although this dataset showed the best correlations, the amplitude ratio exceeded unity at 1.24, indicating a deviation of 0.24 from unity. However, Group 2, the worst scenario, keeps a high amplitude ratio, also of 1.76, but both maintain no delays in the time series.

Despite this, Group 2, as in the eastward component, is the worst-case scenario; the R^2, is the lowest at 0.62, and the RSME is the second lowest with 0.90. The Nash–Sutcliffe efficiency coefficient (NSE), on the northward component in this group, was close to zero. However, the prediction of the FES model is still reliable as the values represent the average of a data series due to the model's method of solving the main mass transport equations and following the analysis of each statistical parameter.

Discussion for FoW results Group 2 is located in a shallow area with a water depth of 15 m, where the model detects signals with higher amplitudes in the eastward and northward direction. This directly impacts the accuracy of the predictions of the model concerning the bathymetry, as reflected in the results.

In contrast, when the model is applied to the location represented by Group 3, with water depths ranging from 37 to 43.1 m, it produces consistent statistics in line with the model's predictions and shows a perfect amplitude ratio. However, despite the similar behaviour between the groups, Group 1's amplitude ratio is 0.24 higher, likely due to the shallower water depths of 29 m, confirming the association between the accuracy of the predictions and the bathymetry. According to this study, a bathymetry of above 40 m is required for FES2014c to provide accurate estimations.

However, the model still shows an overestimation of the data in all groups, where the ideal value would be zero. This could lead to potential variance in the estimated amount of energy that can be extracted from the currents. Nonetheless, this overestimation and the non-phase shift do not appear to be related to the length of the time series, as all values remain consistent. As it is observed in Group 3 and Group 1, with different depths, but with the same BIAS (0.92 ms^{-1}).

Therefore, the accuracy of the predictions of the model can be influenced by the bathymetry, specifically uneven bottom topography (Group 3) and in very shallow areas (Group 2) in the FoW scenario.

Case B - Canadian Archipelago - Nares Strait The following analysis focuses on the Nares Strait site. As stated in the methodology, ADCP data from Arctic Canada was not publicly available, except for this site, which was used for validating FES2014 in Arctic Canadian waters. The statistical analysis of the eastward and northward components is presented in Tables 10 and 11.

Eastward component In general, the data shows a good correlation of 67% on average, but with an underestimation of 1.0 ms^{-1} according to the BIAS, on average between the FES2014c model and the ADCP data.

It was found for DP2 a coefficient of 0.89% and low error values, as indicated by an RMSE of 0.05 ms^{-1}. This is also supported by a high skill score, covering predictions 85% of the time, and an NSE close to unity, 0.79, suggesting a strong correlation. Moreover, the high amplitude ratio of 1.25 indicates some irregularities in the correlation.

On the other hand, DP8 showed the lowest correlation, at 1%, indicating a significant discrepancy between observations and model predictions in the eastward component. This is further supported by a low skill score of 56%, and a negative NSE of −5.89. However, DP8 presents an amplitude ratio closest to unity, at 0.91 and a low RMSE in the correlation of 0.1 ms^{-1}, which suggests that despite present stability in the amplitude, the relationship between the variables is weak.

In general, all the datapoints present an underestimation of around 1 ms^{-1}, as observed in Table 10, based on the calculation of BIAS. Also, no phase shift was found for most of the data points evaluated, except for a leftward trend observed when looking at the phase shift values in DP3, with a difference of −0.04 cycles, while a shift to the right of 0.06 cycles was found for DP7.

Northward component According to Table 11, in this component, the DP3 did not display the highest coefficient of correlation, R^2, but showed a better performance in the other calculated statistics. For example, the RSME was the lowest with 0.11 ms^{-1}, and the skill score was the highest with 79% and had an NSE close to unity (0.41), supporting the good agreement between the model and the ADCP data at this point.

In contrast, it was observed in DP2 that the R^2 value was low, with a correlation coefficient of 23%. Additionally, the RMSE was 0.18 ms^{-1}, which is among the highest values when compared to the other datapoints (ranging from 0.22 ms^{-1} to 0.26 ms^{-1}). This is further supported by the highest underestimation bias of −1.14 ms^{-1}, a high NSE of −21.3, a low amplitude ratio, and skill score values of 34% and 0.31, respectively, indicating that this dataset does not fit the model overall.

Similar to the eastward component, most datapoints show no phase shift, except for DP6, which exhibits a slight offset of 0.05 cycles to the right. Only DP3 and DP4 have positive NSE values (0.41 and 0.07, respectively), suggesting that they are marginally more reliable compared to the overall average observations. These datapoints also have the highest skill scores, ranging from 0.79 to 0.72, respectively. In contrast, the remaining datapoints exhibit negative NSE values, ranging from −98.8 to −1.9, and skill scores between 0.23 and 0.57, with DP7 showing the weakest correlation at 0.23.

Discussion for Canadian Archipelago results The eastward datapoints show a good correlation in most of the calculated statistics, but present an underestimation (1 ms^{-1} to 1.14 ms^{-1}) and high amplitude ratio. This suggests an influence of the model and ADCP data in water depths ranging between 157 m–366 m.

In the case of Nares Strait, measurements using ADCP faced significant challenges during 2003–2006 and 2007–2009. These challenges stemmed from data reliability issues, difficulties in collecting data in polar, under-ice environments, and the visibility of tidal oscillations primarily along the southward direction but not across the channel. It is therefore uncertain whether FES can be used for site selection in this area, based on the available measurements.

In both components, the direction of the model does not align well with the ADCP datapoints, which reflects the challenges encountered during data collection in remote locations that are highly influenced by icing during longer periods.

Despite the datapoints being collected in deep waters, the extreme conditions and high negative results indicate that the model performs worse than the mean of the observations. This implies that the model is not adequately capturing the dynamics of the system. However, these parameters should always be accompanied by other statistics, such as RMSE and BIAS, which in this case helped in selecting the datapoints with better performance and in making informed decisions.

3.2.1. Frequency domain analysis

M2 tidal current ellipses errors were computed from the ADCP locations as described in Section 2.1.1. The right side of Fig. 4 shows the results for the FoW Case. Group 3, maintains the same tendency and low RSME errors of the M2 major axis velocity phase and amplitude,

Table 10
Results of statistics for Canadian Archipelago scenario on the eastward component.

Component	Statistic	D1	D2	D3	D4	D5	D6	D7	D8	D9
Eastward component	R^2	0.85	**0.89**	0.67	0.67	0.79	0.84	0.86	**0.01**	0.50
	RSME (ms^{-1})	0.06	**0.05**	0.15	0.17	0.06	0.10	**0.27**	0.10	0.21
	BIAS (ms^{-1})	**−1.0**	**−1.0**	**−1.0**	**−0.99**	**−1.0**	**−1.0**	**−1.0**	**−1.0**	**−1.0**
	Skill score	0.47	**0.85**	0.69	**0.40**	0.82	0.75	0.56	0.56	0.68
	NSE	−5.96	**0.79**	−5.31	**−24.63**	0.65	0.46	−1.32	−5.89	−5.21
	Phase shift (cycles)	**0.0**	**0.0**	**−0.04**	**0.0**	**0.0**	**0.0**	0.06	**0.0**	**0.0**
	Amplitude ratio	0.35	1.57	0.86	0.33	1.18	1.16	**2.83**	**0.91**	1.20

Table 11
Results of statistics for Canadian Archipelago scenario on the northward component.

Component	Statistic	D1	D2	D3	D4	D5	D6	D7	D8	D9
Northward component	R^2	0.81	**0.23**	0.79	0.60	0.84	0.85	0.51	**0.89**	0.76
	RSME (ms^{-1})	**0.11**	0.18	0.11	0.14	0.22	0.22	0.20	0.13	**0.26**
	BIAS (ms^{-1})	−1.0	**−1.14**	−1.0	−1.0	−1.0	−1.0	**−0.99**	−1.0	−1.01
	Skill score	0.57	0.34	**0.79**	0.72	0.40	0.41	**0.23**	0.52	0.54
	NSE	−1.92	−21.30	**0.41**	0.07	−22.38	−23.42	**−98.83**	−2.77	−12.89
	Phase shift (cycles)	**0.0**	**0.0**	**0.0**	**0.0**	**0.0**	**0.05**	**0.0**	**0.0**	**0.0**
	Amplitude ratio	0.46	0.31	**1.04**	1.18	0.29	0.33	**0.26**	0.35	0.51

with an increment concerning Groups 1 and 2 of 78.5% and 87.31%, respectively.

In contrast, the Canadian Archipelago results show similar directions between the ADCP and the model in the ellipse for DP1 and DP9. However, it was observed that DP3 and DP8, for example, exhibit a low RMSE error of the major axis velocity amplitude and phase, with a value of 66% and 99% in DP9 and DP5.

The results from Fig. 4 of the M2 major axis amplitude-phase and the RSME error confirm that the currents have small-scale variability related to the local bathymetry. However, the FoW area, despite a low range of bathymetry (15 m–43 m), bring out similar shapes of ellipses (ADCP-Model) rather than the Canada archipelago area (157 m–366 m).

Overall, the model shows good agreement with the ADCP at most macro-tidal sites. However, in the Canadian datasets, which represent micro-tidal sites, the discrepancies are large, probably due to extreme conditions in the area and issues with ice affecting data collection.

3.2.2. Assessing tidal stream resource for Nunavut case

In this section, FES is used to evaluate the suitability of sites recommended by MERACAN for energy extraction. Firstly, suitable locations were selected using the MERACAN GIS data, allowing FES to cross-validate and refine the velocity magnitude results obtained from the MERACAN atlas. This part of the study focused solely on the magnitude of tidal currents and wind velocity, without considering separate vector components. The study was divided into 3 zones with notable tidal variations in the currents suitable for energy extraction (see Figs. 6 and 5. These were also selected based on the closeness to populations, for Iqaluit-Kimmirut (Zone 1), three for Naujaat (Repulse Bay) (Zone 2), and two for Igloolik-Sanirajak (Hall Beach) (Zone 3). All with bathymetry depths varying between 14 m–281 m water depth.

Then, it was proceeded to analyse the mean conditions for tidal stream in the selected zones. For zone 1, the highest velocities are close to Quaqtaq between 0.5 ms^{-1} to 1.3 ms^{-1}, in Iqaluit, around 0.3 ms^{-1} to 0.51 ms^{-1}, and in Kangiqsujuaq, the lowest velocities are from 0.1 ms^{-1} to 0.3 ms^{-1}. In Zone 2, the area near Naujaat experiences velocities ranging from 0.1 ms^{-1} to 0.3 ms^{-1}. In Zone 3, the area near Igloolik has velocities of approximately 0.3 ms^{-1} to 0.7 ms^{-1}, while the region from Sanirajak shows velocities ranging from 0.6 ms^{-1} to 1.3 ms^{-1}.

Assessing the offshore wind resource To analyse the opportunities for the development of renewable energy, the zones analysed for tidal stream resources were also assessed for offshore wind data conditions at 50 m. For the offshore wind, in comparison with the tidal stream, the ERA5 model [43] is widely validated, and the accuracy is significantly improved, according to Tahir, et al. (2023), Patel, et al. (2024), amongst others [47,56,78]. Although it has limitations in shallow waters, it offers a continuous time series and lower spatial resolution, making it a reliable model for identifying offshore wind sites.

For the assessment of offshore wind resources, the key factors considered are wind speed as a governing factor, wind power generation (Annual energy production), which gives the potential and the wind direction. A temporal resolution of five years was selected to analyse inter-annual variations. The evaluation was carried out using ERA5 reanalysis data across three zones for Iqaluit - Kimmirut (Zone 1), Naujaat (Repulse Bay) (Zone 2), Igloolik and Sanirajak (Hall Beach) (Zone 3), where tidal stream energy is also applicable, as shown in Fig. 5.

The analysis shows that Zone 1, located near Iqaluit-Kimmirut, experiences wind speeds at 50 m ranging from approximately 3.5 ms^{-1} to 6.7 ms^{-1}. However, certain areas closer to Quaqtaq, with the strongest winds, exhibit significantly higher wind velocities, ranging from 7.8 ms^{-1} to 10.1 ms^{-1}. This is also observed in zone 2, with mean velocities in Cape Dorset about 7.8 ms^{-1} to 10.1 ms^{-1} and at Naujaat around 6.7 ms^{-1} to 7 ms^{-1}. Finally the zone 3 has the lowest velocities between 3.5 ms^{-1} to 6.7 ms^{-1}.

Site selection As detailed in Section 2.1.2, the minimum requirements (cut-in) are 2.5 ms^{-1} for wind and 0.4 ms^{-1} for tidal stream. In both cases, these selected sites accomplish those conditions related to the velocity. Consequently, based on the defined turbines, the data was assessed according to the capacity factor and the required installation depth for each turbine, as the criterion described in Table 1. The power curve, annual energy production (AEP) and capacity factor were calculated for each zone based on the selected offshore wind and tidal stream turbines described in Tables 5 and 6.

As a result, it is necessary to verify first that the requirements related to the bathymetry features were taken into account to assess if the site has the conditions to install the turbine, and to recommend viable solutions. For a fixed wind turbine was between 10 m to 50 m, and for tidal stream, the requirements depend on whether the support structure of the turbine is floating or fixed. Those requirements for fixed

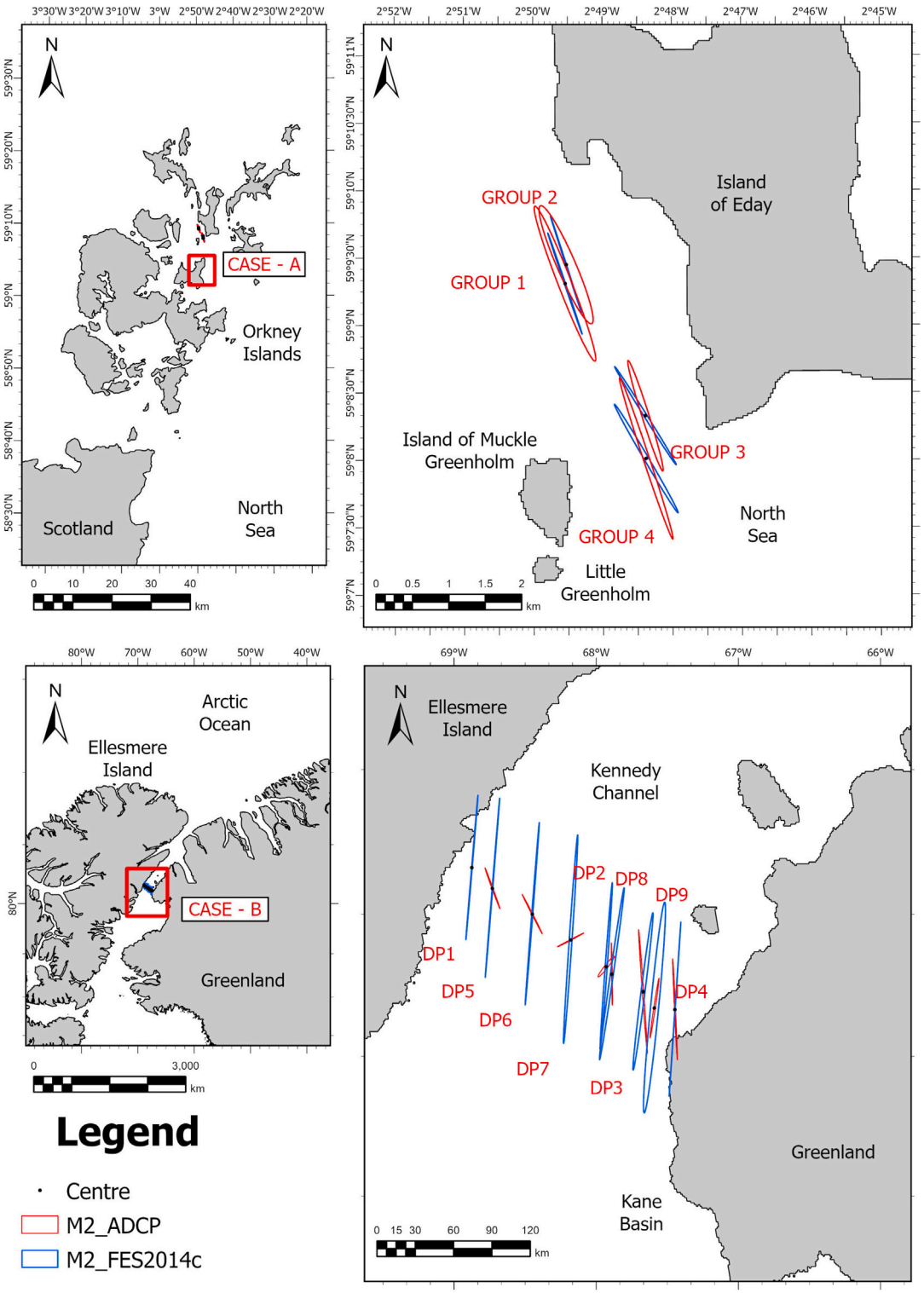

Fig. 4. Ellipse Map for M2 Component at mooring positions.

include a minimum clearance of 8 m from the surface and 5 m from the seabed, with a minimum water depth ranging from 18 m to 50 m. And, depths greater than 4 m for floating structures.

According to Fig. 6, was observed that Sanirajak (19 m), (Zone 3), Iqaluit (47 m), Zone 1, and one site close to Naujaat (Site 3) (41 m), met the minimum requirement in terms of bathymetry in wind. As well as for tidal stream turbines, the sites that matched the fixed turbines were Iqaluit (47 m) and site 3 at Naujaat (41 m). However, for the floating turbines, all the sites are consistent.

In the best scenario, Sites near Kimmirut (286 m) and Naujaat (41 m-158 m) demonstrated compliance with the wind criterion for both 1 MW and 0.5 MW turbines. For the 1 MW option, Site 3 in Naujaat and Kimmirut showed capacity factors between 35% and 49%. For the 0.5 MW turbines, Sites 2 and 3 in Naujaat qualified, reaching slightly higher capacity factors of from 35% up to 52%. However, for the worst

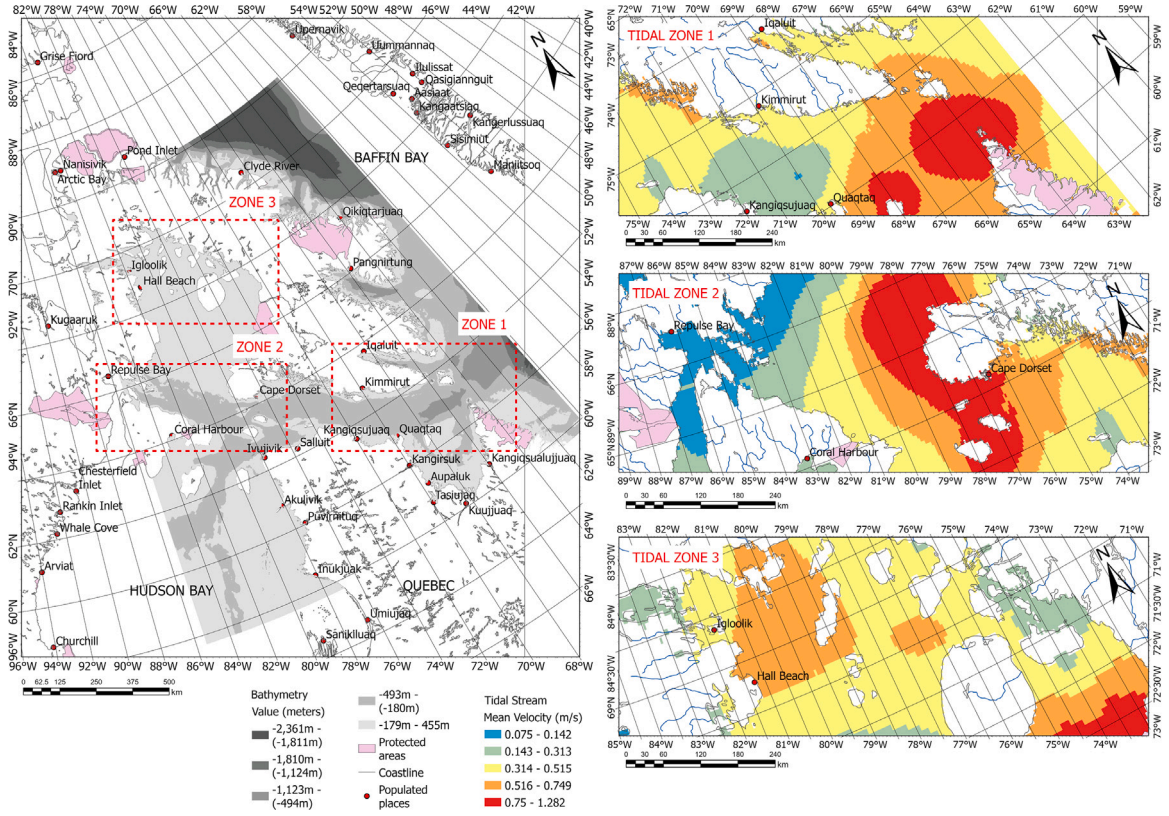

Fig. 5. Mean velocity for offshore wind in the selected zones.

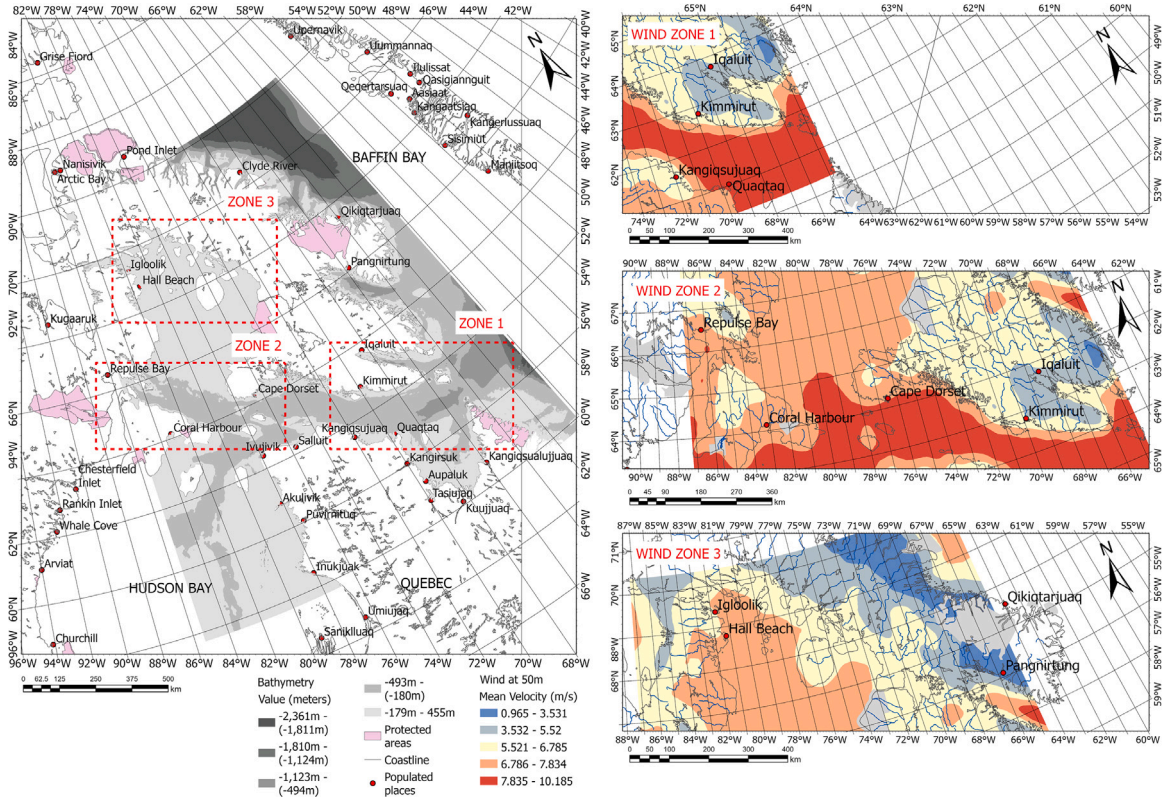

Fig. 6. Mean velocity for tidal stream in the selected zones.

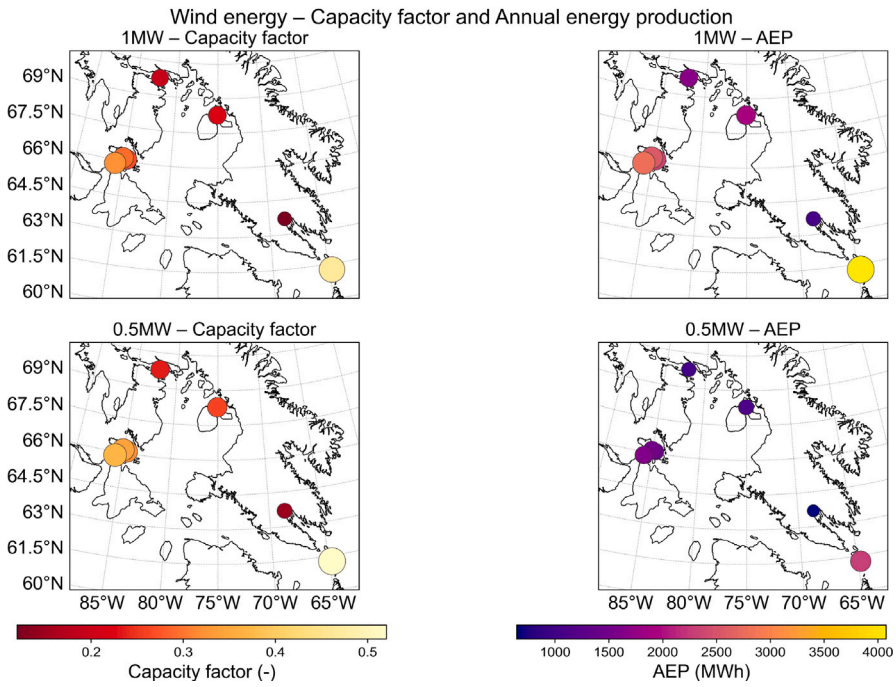

Fig. 7. Capacity factor and Annual energy production for wind in the selected zones.

case scenario, the areas close to Iqaluit and Igloolik did not show the same values as shown by Fig. 7, with the capacity factor between 13% to 24% for both turbines.

For tidal turbines, the capacity factor should range between 16% and 40%. According to Fig. 8, the best scenarios with the highest values were recorded at Site 2 in Naujaat and Kimmirut. The first one (site 2), using the Tocardo 42 kW and Rivgen 25 kW turbines, with a capacity factor of about 30%. Alternatively, the Tidgen 200 kW turbine at Site 2 in Naujaat showed a lower capacity factor of 17%. Similar performance was observed at near Kimmirut with the Tocardo 42 kW turbine, reaching 27%.

In Table 12, the sites suitable for tidal, wind, or both technologies are Kimmirut (Zone 1), Naujaat (Zones 2), and Sanirajak (Zone 3). For wind energy, Naujaat at Site 2 is particularly appropriate, with a bathymetry of 41 m and a capacity factor of 38%, making it a viable location for wind turbine installation, with an annual energy production of 1687.82 MWh (See Fig. 7). Although other sites as Sanirajak, meet the bathymetric requirements, it does not achieve a sufficient capacity factor for effective offshore wind deployment (27%) or at least for the studied devices.

According to Fig. 8, the most suitable sites for tidal stream turbine installations are Naujaat Sites 1 and 2, Naujaat Site 3, and Kimmirut. The Rivgen 25 kW cross-flow turbine was found to be appropriate for Naujaat Sites 1 and 2, yielding estimated annual energy productions of 64.2 MWh and 64.6 MWh, respectively. Similarly, Kimmirut is also suitable for the Rivgen 25 kW turbine, with an annual energy production of 45.3 MWh.

Site 3 at Naujaat stands out as it meets all the assessed parameters, making it suitable for the installation of both tidal and wind energy systems. Specifically, this site supports the Tocardo 42 kW horizontal-axis tidal turbine, in addition to a 0.5 MW wind turbine. As shown in Table 12, this combined setup results in a total annual energy production of 1791.8 MWh.

Although most tidal stream turbines currently operate at sites shallower than 50 m, recent technologies such as TidGen and Tocardo demonstrate that these devices can also be deployed in deeper waters. This evidence indicates that the sites evaluated in this study, including those exceeding 50 m water depth, could realistically accommodate such deep-water turbine systems and therefore should not be disregarded as potential development locations. Accordingly, regions with depths greater than 50 m were retained in the analysis, and Site 3 was selected because its bathymetric characteristics fall within the stated operational envelope of these emerging turbine technologies.

4. Conclusions and future work

This study aimed to assess the accuracy of the FES2014c data assimilation model by comparing it with ADCP measurements at various tidal sites in remote, off-grid regions of the northern Atlantic Ocean, including the FoW in the Orkney Islands, Scotland, and the Canadian Archipelago through the Nares Strait. These evaluations supported identifying tidal sites that could meet the energy needs of remote areas in Nunavut, Canada. The main findings of this work are outlined below:

- According to this analysis, it was found that FES can provide accurate flow characteristics such as flow velocities and tidal phase shift when its use is limited to regions with water depths higher than 40 m.
- The amplitude ratio is, however, affected by the bathymetry. It was noted that in areas with low-resolution data, the accuracy of the amplitude ratio decreases, which impacts the interpretation of ocean dynamics.
- Traditional metrics such as the correlation coefficient, RMSE, and R^2 may suggest strong model agreement; however, they are not sufficient to evaluate performance reliably. This study demonstrates that additional metrics can reveal limitations that remain hidden when relying solely on common statistics. Therefore, a multi-metric evaluation approach is essential for an overall picture of the model.
- This research also highlights the need to validate regional conditions when applying global data assimilation models such as FES2014c. The comparison between Canada and FoW shows that, particularly under low-velocity conditions, a multi-metric approach exposes relevant differences between the eastward and northward tidal components that are not identified when only traditional metrics are applied.

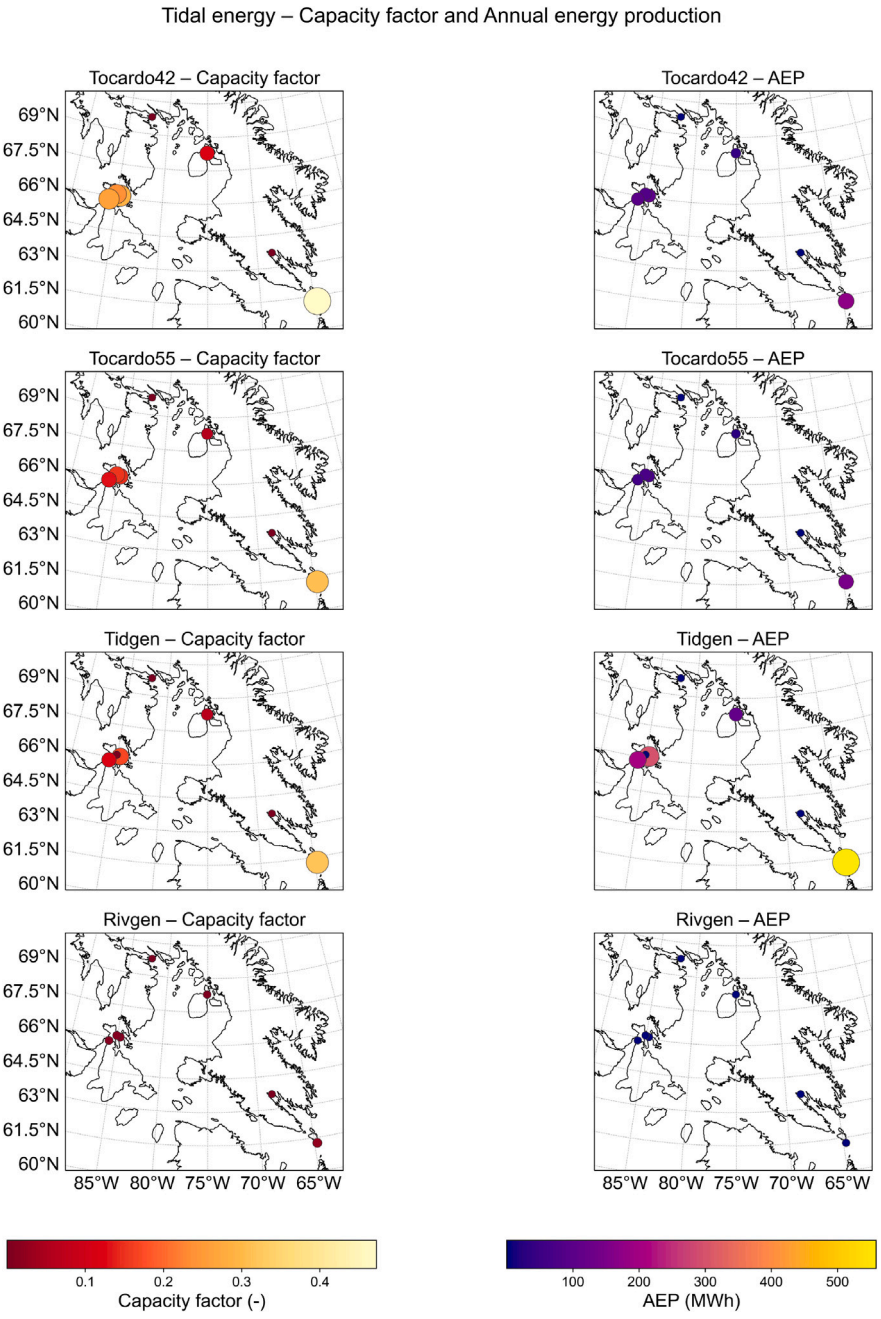

Fig. 8. Capacity factor and Annual energy production for tidal stream in the selected zones.

Table 12
Site assessment and recommendations by zone.

Parameters	Zone 1		Zone 2			Zone 3	
	Iqaluit	Kimmirut	Naujaat 1	Naujaat 2	Naujaat 3	Igloolik	Sanirajak
Site recommendation	None	Tidal, Rivgen-25 kW, 20%, 45.3 MWh	Tidal, Rivgen-25 kW, 29%, 64.2 MWh	Tidal, Rivgen-25 kW, 29%, 64.6 MWh	Both, 0.5 MW, 38% and Tocardo42 kW, 28% - 1791. 8 MWh (Combined Tidal + Wind)	None	None
Bathymetry (metres)	47	286	158	91	41	6	19

- Although the model demonstrates strong temporal skill for both validation cases in Scotland and Canada, the magnitude bias identified through the RMSE analysis highlights the need for further refinement. Future work will apply local calibration or downscaling factors to improve accuracy and strengthen the reliability of threshold-based site classification.

This analysis provided valuable insights to support the development and implementation of renewable energy projects in Nunavut areas, with specific recommendations for the following sites:

- For the selected locations of Kimmirut and Naujaat (sites 1 and 2), offshore wind energy was not chosen due to deep waters (≥50 m) and calculated capacity factors of less than 30%.
- The results suggest that Kimmirut and three sites at the Naujaat area are suitable to locate tidal stream turbines such as the Rivgen25kW and Tocardo 42 kW, with a capacity factor ranging from 20%–29%, and an annual energy production (AEP) between 45.3 MWh (Kimmirut) and 1791.8 MWh (combined tidal and wind AEP for Site 3 at Naujaat).
- Site 3 in Naujaat was identified as a suitable location for the deployment of both tidal and offshore wind energy, with capacity factors of 28% and 38%, respectively. The combined annual energy production was estimated at approximately 1791.8 MWh.
- Other areas suggested for further exploration, due to their potential for wind and tidal stream energy based on MERACAN atlas, including Cape Dorset, Kinngait, Rankin Inlet, and Chesterfield Inlet. Moreover, this methodology could be replicated in other regions dependent on fossil fuels or reliant on hydraulic systems, such as tropical areas, even where tidal stream and wind velocities are lower and access to field data is limited, as was done in this investigation.
- The navigational, environmental, or socio-economic constraints are present in the area; we acknowledge that these factors will ultimately influence the practical developability of the identified sites for maritime spatial planning. However, a techno-economic evaluation and marine spatial planning analysis were not included in the present study, but represent important next steps for future research to determine the deployment and site prioritisation.

CRediT authorship contribution statement

Marianella Bolivar-Carbonell: Writing – review & editing, Writing – original draft, Visualization, Validation, Software, Methodology, Investigation, Formal analysis, Data curation, Conceptualization. **Matthew Lewis:** Writing – review & editing, Methodology, Data curation. **Roberto Guerrero-Gomez:** Visualization, Software. **Stephanie Ordonez-Sanchez:** Writing – review & editing, Writing – original draft, Supervision, Methodology, Conceptualization.

Declaration of Generative AI and AI-assisted technologies in the writing process

During the preparation of this work, the authors used Grammarly and ChatGPT to improve the clarity and flow of the text. After using the tool, the authors reviewed and edited the content as needed and take(s) full responsibility for the content of the published article.

Declaration of competing interest

The authors declare that they have no known competing financial interests or personal relationships that could have appeared to influence the work reported in this paper.

Acknowledgements

The authors would like to acknowledge the support of the project "Renewable Energy Microgrid Integration for Remote, Off-grid Cabins in Nunavut, funded by the Canada-Inuit Nunangat-United Kingdom Arctic Research Programme. S Ordonez-Sanchez would also like to thank the Royal Academy of Engineering, United Kingdom for its support through the IF-2425-19-AI174 fellowship.

Data availability

Data will be made available on request.

References

[1] Sovacool BK. The political economy of energy poverty: A review of key challenges. Energy Sustain Dev 2012;16(3):272–82. http://dx.doi.org/10.1016/j.esd.2012.05.006, URL https://www.sciencedirect.com/science/article/pii/S0973082612000373.

[2] LiVecchi A, Copping A, Jenne D, Gorton A, Preus R, Gill G, Robichaud R, Green R, Geerlofs S, Gore S, Hume D, Mc Shane W, Schmaus C, Spence H. Powering the blue economy, exploring opportunities for marine renewable energy in maritime markets. U.S. Department of Energy, Office of Energy Efficiency and Renewable Energy. Washington, D.C.; 2019.

[3] Goward Brown AJ, Lewis M, Barton BI, Jeans G, Spall SA. Investigation of the modulation of the tidal stream resource by ocean currents through a complex tidal channel. J Mar Sci Eng 2019;7(10). http://dx.doi.org/10.3390/jmse7100341, URL https://www.mdpi.com/2077-1312/7/10/341.

[4] Lorafe L, Taboada Evelyn B. Demystifying the authentic attributes of electricity-poor populations: The electrification landscape of rural off-grid island communities in the Philippines. Energy Policy 2020;145(C).

[5] Blechinger P, Cader C, Bertheau P, Huyskens H, Seguin R, Breyer C. Global analysis of the techno-economic potential of renewable energy hybrid systems on small islands. Energy Policy 2016;98:674–87. http://dx.doi.org/10.1016/j.enpol.2016.03.043, URL https://www.sciencedirect.com/science/article/pii/S0301421516301471.

[6] Weisser D. On the economics of electricity consumption in small island developing states: a role for renewable energy technologies? Energy Policy 2004;32(1):127–40. http://dx.doi.org/10.1016/S0301-4215(03)00047-8, URL https://www.sciencedirect.com/science/article/pii/S0301421503000478.

[7] Brouwer AS, van den Broek M, Seebregts A, Faaij A. Impacts of large-scale intermittent renewable energy sources on electricity systems, and how these can be modeled. Renew Sustain Energy Rev 2014;33:443–66. http://dx.doi.org/10.1016/j.rser.2014.01.076, URL https://www.sciencedirect.com/science/article/pii/S1364032114000987.

[8] Kirby K, Fu S, Ordonez-Sanchez S, Lavery G, Bolivar-Carbonell M, Banister C, Okalik-Musgroveand J, Johnstone C, Rennie C. Harnessing hydrokinetic energy for enhanced energy resilience in the arctic communities of Canada. In: Pan-American marine energy conference. 2024, p. 13.

[9] Cornnet A. Inventory of Canada's marine renewable energy resources. Tech. rep., Canadian Hydraulics Centre, National Research Council Canada; 2006.

[10] Pinto H, Gates ID. Why is it so difficult to replace diesel in Nunavut, Canada? Renew Sustain Energy Rev 2022;157:112030. http://dx.doi.org/10.1016/j.rser.2021.112030, URL https://www.sciencedirect.com/science/article/pii/S1364032121012922.

[11] Start-up company pitches tidal power for Nunavut. 2014.

[12] Jarquin-Laguna A, Ordonez-Sanchez S. Utilising tidal stream energy to drive seawater reverse osmosis desalination processes. In: 14th European wave and tidal energy conference. EWTEC 2021, 2021, p. 11.

[13] Junqiang X, Roger F, Binliang L. Numerical model assessment of tidal stream energy resources in the Severn Estuary, UK. Proc Inst Mech Eng A 2010;1:1–15. http://dx.doi.org/10.1243/09576509JPE938.

[14] Chowdhury MS, Rahman KS, Selvanathan V, Nuthammachot N, Suklueng M, Mostafaeipour A, Habib A, Akhtaruzzaman M, Amin N, Techato K. Current trends and prospects of tidal energy technology. Environ Dev Sustain 2021;23. http://dx.doi.org/10.1007/s10668-020-01013-4.

[15] Sun Y, Li Y, Wang R, Ma R. Assessing the national synergy potential of onshore and offshore renewable energy from the perspective of resources dynamic and complementarity. Energy 2023;279:128106. http://dx.doi.org/10.1016/j.energy.2023.128106, URL https://www.sciencedirect.com/science/article/pii/S0360544223015001.

[16] Elshafei B, Peña A, Xu D, Ren J, Badger J, Pimenta FM, Giddings D, Mao X. A hybrid solution for offshore wind resource assessment from limited onshore measurements. Appl Energy 2021;298:117245. http://dx.doi.org/10.1016/j.apenergy.2021.117245, URL https://www.sciencedirect.com/science/article/pii/S0306261921006656.

[17] Patel R, Nagababu G, Kachhwaha SS, Surisetty VAK. A revised offshore wind resource assessment and site selection along the Indian coast using ERA5 near-hub-height wind products. Ocean Eng 2022;254:111341. http://dx.doi.org/10.1016/j.oceaneng.2022.111341, URL https://www.sciencedirect.com/science/article/pii/S0029801822007314.

[18] Zaron ED, Elipot S. An assessment of global ocean barotropic tide models using geodetic mission altimetry and surface drifters. Am Meteorol Soc 2021. http://dx.doi.org/10.1175/JPO-D-20, URL https://doi.org/10.1175/JPO-D-20-.

[19] Lyard F, Lefevre F, Letellier T, Francis O. Modelling the global ocean tides: Modern insights from FES2004. Ocean Dyn 2006;56:394–415. http://dx.doi.org/10.1007/s10236-006-0086-x.

[20] Lyard FH, Allain DJ, Cancet M, Carrère L, Picot N. FES2014 global ocean tide atlas: Design and performance. Ocean Sci 2021;17:615–49. http://dx.doi.org/10.5194/os-17-615-2021.

[21] Hallberg R, Rhines P. Buoyancy-driven circulation in an ocean basin with isopycnals intersecting the sloping boundary. J Phys Oceanogr 1996;26. http://dx.doi.org/10.1175/1520-0485(1996)026<0913:BDCIAO>2.0.CO;2.

[22] Simmons HL, Hallberg RW, Arbic BK. Internal wave generation in a global baroclinic tide model. Deep-Sea Res II 2004;51:3043–68. http://dx.doi.org/10.1016/j.dsr2.2004.09.015.

[23] Jayne SR, Laurent LS. Parameterizing tidal dissipation over rough topography. Geophys Res Lett 2001;28:811–4. http://dx.doi.org/10.1029/2000GL012044.

[24] Green JA, Nycander J. A comparison of tidal conversion parameterizations for tidal models. J Phys Oceanogr 2013;43. http://dx.doi.org/10.1175/JPO-D-12-023.1.

[25] Egbert GD, Bennett AF, Foreman MG. TOPEX/POSEIDON tides estimated using a global inverse model. J Geophys Res 1994;99. http://dx.doi.org/10.1029/94jc01894.

[26] Davies A, Jones J. A three dimensional model of the M2, S2, N2, K1 and O1 tides in the Celtic and Irish seas. Prog Oceanogr 1992;29(3):197–234. http://dx.doi.org/10.1016/0079-6611(92)90004-J, URL https://www.sciencedirect.com/science/article/pii/007966119290004J.

[27] Davies AM. A three-dimensional model of the Northwest European Continental Shelf, with application to the M4 tide. J Phys Oceanogr 1986;16.

[28] Luyten JR, Stommel HM. Comparison of M2 tidal currents observed by some deep moored current meters with those of the Schwiderski and Laplace models. Deep Sea Res A 1991;38:S573–89. http://dx.doi.org/10.1016/s0198-0149(12)80024-0.

[29] Liu X, Chen Z, Si Y, Qian P, Wu H, Cui L, Zhang D. A review of tidal current energy resource assessment in China. Renew Sustain Energy Rev 2021;145:111012. http://dx.doi.org/10.1016/j.rser.2021.111012, URL https://www.sciencedirect.com/science/article/pii/S1364032121003026.

[30] Wen Y, Lin P. Exploitation potential of tidal current energy in Southern China seas. Energy Convers Manage 2022;267:115901. http://dx.doi.org/10.1016/j.enconman.2022.115901, URL https://www.sciencedirect.com/science/article/pii/S0196890422006975.

[31] Dai P, Huang Z, Zhang J. A modelling study of the tidal stream resource around Zhoushan Archipelago, China. Renew Energy 2023;218:119234. http://dx.doi.org/10.1016/j.renene.2023.119234, URL https://www.sciencedirect.com/science/article/pii/S0960148123011497.

[32] Chen J, Dai C, Wen B, Ren L, Li D, Jin X. Tidal current energy resources assessment in Zhoushan Archipelago, China. Int J Green Energy 2024;21(10):2239–50. http://dx.doi.org/10.1080/15435075.2023.2299939.

[33] Dushaw BD, Egbert GD, Worcester PF, Cornuelle BD, Howe BM, Metzger K. A TOPEX/POSEIDON global tidal model (TPXO.2) and barotropic tidal currents determined from long-range acoustic transmissions. Prog Oceanogr 1997;40(1–4):337–67.

[34] Ray RD, Eanes RJ, Egbert GD, Pavlis NK. Error spectrum for the global M2 ocean tide. Geophys Res Lett 2001.

[35] Walton T. Tidal velocity asymmetry at inlets. Usace 2002.

[36] Neill SP, Scourse JD, Uehara K. Evolution of bed shear stress distribution over the northwest European shelf seas during the last 12,000 years. Ocean Dyn 2010;60:1139–56. http://dx.doi.org/10.1007/s10236-010-0313-3.

[37] Stammer D, Ray RD, Andersen OB, Arbic BK, Bosch W, Carrère L, Cheng Y, Chinn DS, Dushaw BD, Egbert GD, Erofeeva SY, Fok HS, Green JA, Griffiths S, King MA, Lapin V, Lemoine FG, Luthcke SB, Lyard F, Morison J, Müller M, Padman L, Richman JG, Shriver JF, Shum CK, Taguchi E, Yi Y. Accuracy assessment of global barotropic ocean tide models. Rev Geophys 2014;52:243–82. http://dx.doi.org/10.1002/2014RG000450.

[38] Ranji Z, Hejazi K, Soltanpour M, Allahyar MR. Inter-comparison of recent tide models for the Persian gulf and oman sea. Coast Eng Proc 2017;9. http://dx.doi.org/10.9753/icce.v35.currents.9.

[39] Cancet M, Lyard F, Griffin D, Carrère L, Picot N. Assessment of the FES2014 tidal currents on the shelves around Australia. Tech. rep., Noveltis; 2017.

[40] Howe BM, Arbic BK, Aucan J, Barnes CR, Bayliff N, Becker N, Butler R, Doyle L, Elipot S, Johnson GC, Landerer F, Lentz S, Luther DS, Müller M, Mariano J, Panayotou K, Rowe C, Ota H, Song YT, Thomas M, Thomas PN, Thompson P, Tilmann F, Weber T, Weinstein S. SMART cables for observing the global ocean: Science and implementation. Front Mar Sci 2019;6. http://dx.doi.org/10.3389/fmars.2019.00424, URL https://www.frontiersin.org/journals/marine-science/articles/10.3389/fmars.2019.00424.

[41] Carrere L, Arbic BK, Dushaw B, Egbert G, Erofeeva S, Lyard F, Ray RD, Ubelmann C, Zaron E, Zhao Z, Shriver JF, Buijsman MC, Picot N. Accuracy assessment of global internal-tide models using satellite altimetry. Ocean Sci 2021;17:147–80. http://dx.doi.org/10.5194/os-17-147-2021.

[42] Timko PG, Arbic BK, Richman JG, Scott RB, Metzger EJ, Wallcraft AJ. Skill testing a three-dimensional global tide model to historical current meter records. J Geophys Res: Ocean 2013;118:6914–33. http://dx.doi.org/10.1002/2013JC009071.

[43] Hersbach, Bell, Berrisford, Biavati, Horányi, Sabater M, Nicolas, Peubey, Radu, Rozum, Schepers, Simmons, Soci, Dee, Thépaut J-N. ERA5 hourly data on single levels from 1940 to present. Tech. rep., Copernicus Climate Change Service (C3S) Climate Data Store (CDS); 2023, [Accessed 01 January 2025].

[44] Lewis M, O'Hara Murray R, Fredriksson S, Maskell J, de Fockert A, Neill SP, Robins PE. A standardised tidal-stream power curve, optimised for the global resource. Renew Energy 2021;170:1308–23. http://dx.doi.org/10.1016/j.renene.2021.02.032, URL https://www.sciencedirect.com/science/article/pii/S0960148121001993.

[45] Statista I. Average capacity factor for offshore wind power worldwide from 2010 to 2023 [graph]. Tech. rep., IRENA; 2024, Retrieved June 20, 2025, from https://www.statista.com/statistics/1368679/global-offshore-wind-capacity-factor/.

[46] Coles D, Angeloudis A, Greaves D, Hastie G, Lewis M, Mackie L, McNaughton J, Miles J, Neill S, Piggott M, Risch D, Scott B, Sparling C, Stallard T, Thies P, Walker S, White D, Willden R, Williamson B. A review of the UK and British Channel Islands practical tidal stream energy resource. Proc R Soc A 2021;477(2255):20210469. http://dx.doi.org/10.1098/rspa.2021.0469, URL https://royalsocietypublishing.org/doi/abs/10.1098/rspa.2021.0469. arXiv:https://royalsocietypublishing.org/doi/pdf/10.1098/rspa.2021.0469.

[47] Patel M. The impact of real-world constraints on tidal stream energy resource assessments [Ph.D. thesis], University of Oxford; 2024.

[48] Cousineau J. Inventory and assessment of tidal energy resources near northern communities. Tech. rep., National Research Council Canada; 2020.

[49] Yu Z, Wu J, Chen X. An approach to revising the climate forecast system reanalysis rainfall data in a sparsely-gauged mountain basin. Atmos Res 2019;220:194–205. http://dx.doi.org/10.1016/j.atmosres.2019.01.014, URL https://www.sciencedirect.com/science/article/pii/S0169809518308068.

[50] Vega-Durán J, Escalante-Castro B, Canales FA, Acuña GJ, Kaźmierczak B. Evaluation of areal monthly average precipitation estimates from MERRA2 and ERA5 reanalysis in a Colombian caribbean basin. Atmosphere 2021;12(11). URL https://www.mdpi.com/2073-4433/12/11/1430.

[51] Nash J, Sutcliffe J. River flow forecasting through conceptual models part I — A discussion of principles. J Hydrol 1970;10(3):282–90. http://dx.doi.org/10.1016/0022-1694(70)90255-6, URL https://www.sciencedirect.com/science/article/pii/0022169470902556.

[52] Chen F, Li X. Evaluation of IMERG and TRMM 3b43 monthly precipitation products over mainland China. Remote Sens 2016;8. http://dx.doi.org/10.3390/rs8060472.

[53] Legrand C. Assessment of tidal energy resource: marine renewable energy guides. Tech. rep., The European Marine Energy Centre Limited; 2009.

[54] Pawlowicz R, Beardsley B, Lentz S. Classical tidal harmonic analysis including error estimates in MATLAB using ttide. Comput Geosci 2002.

[55] Griffin DA, Herzfeld M, Hemer M, Engwirda D. Australian tidal currents – assessment of a barotropic model (COMPAS v1.3.0 rev6631) with an unstructured grid. Geosci Model Dev 2021;14(9):5561–82. http://dx.doi.org/10.5194/gmd-14-5561-2021, URL https://gmd.copernicus.org/articles/14/5561/2021/.

[56] ul Rehman Tahir Z, Abdullah M, Ahmad S, Kanwal A, Farhan M, Saeed UB, Ali T, Amin I. An approach to assess offshore wind power potential using bathymetry and near-hub-height reanalysis data. Ocean Eng 2023;280:114458. http://dx.doi.org/10.1016/j.oceaneng.2023.114458, URL https://www.sciencedirect.com/science/article/pii/S0029801823008429.

[57] Liu L, Wu M, Mao Y, Zheng L, Xue M, Bing L, Liang F, Liu J, Liu B. Offshore wind energy potential in Shandong Sea of China revealed by ERA5 reanalysis data and remote sensing. J Clean Prod 2024;464:142745. http://dx.doi.org/10.1016/j.jclepro.2024.142745, URL https://www.sciencedirect.com/science/article/pii/S0959652624021930.

[58] Kardakaris K, Boufidi I, Soukissian T. Offshore wind and wave energy complementarity in the greek seas based on ERA5 data. Atmosphere 2021;12(10). http://dx.doi.org/10.3390/atmos12101360, URL https://www.mdpi.com/2073-4433/12/10/1360.

[59] Gualtieri G. Reliability of ERA5 reanalysis data for wind resource assessment: A comparison against tall towers. Energies 2021;14(14). http://dx.doi.org/10.3390/en14144169, URL https://www.mdpi.com/1996-1073/14/14/4169.

[60] Zhai R, Huang C, Yang W, Tang L, Zhang W. Applicability evaluation of ERA5 wind and wave reanalysis data in the south China sea. J Ocean Limnol 2023;41(2):495–517.

[61] Alkhalidi M, Al-Dabbous A, Al-Dabbous S, Alzaid D. Evaluating the accuracy of the ERA5 model in predicting wind speeds Across Coastal and offshore regions. J Mar Sci Eng 2025;13(1). http://dx.doi.org/10.3390/jmse13010149, URL https://www.mdpi.com/2077-1312/13/1/149.

[62] Cheynet E, Diezel JM, Haakenstad H, Breivik Ø, Peña A, Reuder J. Tall wind profile validation using lidar observations and hindcast data. Wind Energy Sci Discuss 2024;2024:1–29.

[63] https://en.wind-turbine-models.com/turbines/67-enercon-e-40-5.40.

[64] https://en.wind-turbine-models.com/turbines/396-an-bonus-1000-54.

[65] Verbeek M, Labeur R, Uijttewaal W. The performance of a weir-mounted tidal turbine: An experimental investigation. Renew Energy 2021;168:64–75. http://dx.doi.org/10.1016/j.renene.2020.12.013, URL https://www.sciencedirect.com/science/article/pii/S096014812031939X.

[66] https://tocardo.com/hydro-turbines/.

[67] McGlynn J. River hydrokinetic energy overview. In: ESMAP training program, IFC, 17th June 2014. 2014.

[68] Cavagnaro RJ, Polagye B, Thomson J, Brian Fabien DF, Kilcher L, Donegan J, McEntee J. Emulation of a hydrokinetic turbine to assess control and grid integration. In: Proceedings of the 11th European wave and tidal energy conference 6-11th sept 2015, Nantes, France. 2015.

[69] Jarlath McEntee P. Preliminary turbine hydrodynamic design – DE-EE0007820 – Advanced TIDGEN®. Tech. rep., Ocean Renewable Power Company; 2017.

[70] Jarlath McEntee P. D3.3 - final subsystem design and development plan -DE-EE0007820– Advanced TIDGEN®. Tech. rep., Ocean Renewable Power Company; 2018.

[71] Jarlath McEntee P. D7.2.9 final system design-DE-EE0007820 – Advanced TIDGEN®. Tech. rep., Ocean Renewable Power Company; 2018.

[72] GEBCO compilation group (2024) GEBCO 2024 grid (http://dx.doi.org/10.5285/1c44ce99-0a0d-5f4f-e063-7086abc0ea0f).

[73] Sellar BG. Support document for the ReDAPT tidal site environmental data archive an introduction to the redapt tidal project environmental data set v2.0. Tech. rep., Institute for Energy Systems, School of Engineering, University ofd Edinburgh; 2016.

[74] Martinez R, Ordonez-Sanchez S, Allmark M, Lloyd C, O'Doherty T, Germain G, Gaurier B, Johnstone C. Analysis of the effects of control strategies and wave climates on the loading and performance of a laboratory scale horizontal axis tidal turbine. Ocean Eng 2020;212:107713. http://dx.doi.org/10.1016/j.oceaneng.2020.107713, URL https://www.sciencedirect.com/science/article/pii/S0029801820307010.

[75] O'Doherty T. Dynamic loadings on turbines in a tidal array (DyLoTTA). Tech. rep., Cardiff University - Sch of Engineering; 2016.

[76] Muenchow A. Canadian archipelago throughflow study: ADCP moorings 2003-06. Tech. rep., Arctic Data Center; 2013.

[77] Muenchow A. Canadian archipelago throughflow study: ADCP moorings 2007-09. Tech. rep., NSF Arctic Data Center; 2014.

[78] Ahmad S, Abdullah M, Kanwal A, Tahir ZuR, Saeed UB, Manzoor F, Atif M, Abbas S. Offshore wind resource assessment using reanalysis data. Wind Eng 2022;46(4):1173–86.